JOURNAL OF PROPULSION AND POWER
Vol. 25, No. 6, November–December 2009

Catalyzed Ignition of Using Methane/Hydrogen Fuel in a Microtube for Microthruster Applications

Christopher A. Mento,* Chih-Jen Sung,† and Alfonso F. Ibarreta‡
Case Western Reserve University, Cleveland, Ohio 44106
and
Steven J. Schneider§
NASA John H. Glenn Research Center at Lewis Field, Cleveland, Ohio 44135

DOI: 10.2514/1.42592

Catalyzed combustion of propellants in a microtube serves as a model of a microthruster that has potential applications for micropropulsion for small satellites/spacecraft. The effect of hydrogen addition on fuel-rich methane/oxygen ignition within a 0.40-mm-diam platinum microtube is investigated experimentally. All tests are conducted in a vacuum chamber with an ambient pressure of 0.0136 atm to simulate high-altitude conditions. Experimental results show that the critical temperature needed to catalytically lightoff fuel-rich methane/oxygen mixtures is reduced by the addition of small amounts of hydrogen to the mixture. Two-stage ignition phenomena are observed for low levels of hydrogen addition (2–7% by volume), with the first and second ignition conditions corresponding to the reactions of hydrogen and methane, respectively. The effects of changing flow rate (residence time), equivalence ratio, and amount of hydrogen addition on the critical ignition temperature are investigated. The ability of the catalyst to sustain chemical reactions once the input power is turned off is also explored and, for most cases, self-sustainability is realized. Various microtube performance parameters are estimated for all experiments, which include thrust, specific impulse, and power required to ignite reactions within the microtube.

I. Introduction

THERE has been a recent interest from the military, commercial, and academic sectors in developing spacecraft that weigh less than 100 kg. Potential applications for these spacecraft include high-resolution imaging, formation flying within a constellation, and on-orbit repair of larger spacecraft [1]. The benefits of using small spacecraft for missions include a reduction in cost, an increase in launch rate, and a decrease in mission risk [2]. With the need for smaller spacecraft also comes a corresponding need for a scaled-down propulsion system. The propulsion system of a micro- or nanospacecraft will be required to produce thrust in the 1–10 mN range to provide high maneuverability, orbit injection correction, and drag compensation [1].

Of the two types of micropropulsion systems available, chemical or electrical, electrical systems are currently the most advanced and have proven flightworthy in a number of missions. The electrical systems produce thrust by either accelerating ionized particles through an electric field or by electrically heating the propellant and then expanding it through a nozzle. Examples of current electric micropropulsion systems today include resistojets [3,4], field emission electric propulsion thrusters [5], vaporizing liquid thrusters [6,7], Hall-effect thrusters [2,8], pulsed plasma thrusters [9,10], and colloid thrusters [11,12]. There is also a need, however, to develop efficient chemical micropropulsion systems. Chemical micropropulsion offers two main advantages over electrical micropropulsion: 1) the ability to use high specific energy fuels, and 2) the expected lower power requirements needed for operation. Recent work has focused on monopropellants [13,14], bipropellants [15–18], and solid [19,20] and hybrid [21] rockets. A review of studies in chemical micropropulsion can be found in [22,23].

Although there are many attractive features of chemical micropropulsion, there are also many design challenges that are present when the size of the combustor is reduced. Because of the low Reynolds numbers at small characteristic dimensions, frictional losses become large, and thus the amount of pumping needed to flow reactants through the system must be increased [24]. As the combustor size is decreased, the surface-to-volume ratio is increased, and because heat release is proportional to volume and heat loss is proportional to surface area, the heat loss term may become dominant. At small length scales, quenching of the chemical reactions may occur. With a decrease in chamber length, the residence time of the combustor will be reduced, whereas the chemical reaction time is independent of thruster size. For microcombustors, the residence time may therefore be on the order of or smaller than the chemical reaction time, which can result in incomplete or suppressed combustion [25].

The use of catalytic combustion is an efficient way to mitigate many of the problems associated with microcombustion. Because the main reaction occurs at the surface of the catalyst, a high surface-to-volume ratio favors catalytic combustion. The use of catalytic combustion can therefore help overcome the large heat losses at the small scale and allow small combustor sizes to be realized. Because catalytic combustion allows operation in either ultrarich or ultralean conditions beyond the classical gas-phase flammability limits, the product temperatures associated with catalytic combustion can be lower than typical flame temperatures, and thus damage to the combustor walls can be minimized.

Bipropellant mixtures of CH_4/O_2 are chosen for this study due to their importance in future manned missions to Mars. The need for in situ resource utilization, to reduce the total amount of propellant carried from Earth, has been emphasized. Methane can be produced

Received 5 December 2008; revision received 5 August 2009; accepted for publication 8 August 2009.

*Graduate Student, Department of Mechanical and Aerospace Engineering; currently Technical Development Engineer, Flow Sciences; cmento@flowsciences.com. Member AIAA.

†Professor, Department of Mechanical and Aerospace Engineering; currently Professor, Department of Mechanical Engineering, University of Connecticut, Storrs, Connecticut 06269; cjsung@engr.uconn.edu. Associate Fellow AIAA (Corresponding Author).

‡Research Associate, Department of Mechanical and Aerospace Engineering; currently Associate, Exponent; aibarreta@exponent.com.

§Aerospace Engineer, Multidisciplinary Design, Analysis, and Optimization Branch; Steven.J.Schneider@grc.nasa.gov. Associate Fellow AIAA.

from carbon dioxide, which is abundant in the Martian atmosphere, and hydrogen can either be extracted from Martian ice water or brought from Earth. Methods for methane production using these two gases include the Sabatier process, reverse water-gas shift, and solid oxide electrolysis [26,27]. NASA's long-term plan for a manned mission to Mars calls for the use of liquid methane/oxygen mixtures as propellants for an ascent vehicle from the surface of Mars to a Martian orbit.[¶] The current study involves developing a microthruster for space-based applications that would use propellants already being produced in the Martian environment.

Previous work involving catalytic combustion in platinum microtubes primarily focused on either hydrogen [16,17] or methane [18] as the fuel. Methane fuel offers the advantage of being easily storable at low pressures, making it ideal for propulsion systems intended for long-term use. Hydrogen fuel, however, is easier to ignite and has superior performance abilities. Previous studies [16–18] concluded that thrust on the order of 1–10 mN can be achieved using catalytic platinum microtubes with inside diameters of 0.40 and 0.80 mm. For hydrogen/oxygen mixtures, it was observed that, for equivalence ratios between 6.7 and 13.3 at 0.0136 atm ambient conditions, the critical temperatures needed for lightoff were in the range of 410–480 K. For methane/oxygen mixtures between equivalence ratios 6 and 10 at the same ambient pressure conditions the critical temperatures ranged from 651 to 839 K. Thus, it is seen that pure methane/oxygen mixtures require a substantially higher preheat temperature to obtain catalytic ignition than hydrogen/oxygen mixtures.

An exploratory study was also carried out in [18] to examine the effects of adding hydrogen to methane/oxygen mixtures. It was found that the ignition temperature with hydrogen addition can be substantially reduced. However, for all cases studied in [18], a constant H_2 mass flow rate of 0.0001 g/s was added to the rich CH_4/O_2 mixtures. Therefore, further systematic investigation over a wide range of hydrogen addition is warranted. The current work involves studying the effects of the addition of hydrogen to methane/oxygen mixtures in an attempt to use the high reactivity of hydrogen so that methane can be ignited at a lower temperature. A 0.40 mm platinum tube is used for all experiments and, through the use of a vacuum chamber, the ambient pressure is reduced to 0.0136 atm so as to simulate high-altitude conditions. Specifically, the focus of the work is on ignition characteristics and microthruster performance parameters at varying levels of hydrogen addition. The experiments are carried out by holding the overall equivalence ratio constant, while varying the fuel mixture conditions from pure methane to pure hydrogen. Because most previous work [28–31] involving hydrogen-assisted catalytic combustion of hydrocarbons has focused on fuel-lean mixtures, this current study of fuel-rich mixtures contributes a complementary set of ignition data. The following sections detail the experimental setup and present the results of the study.

II. Experimental Setup

Figure 1 shows the schematic of the present experimental setup. The platinum microtube used for all ignition/performance characterization experiments has an inner diameter of 0.40 mm, a wall thickness of 0.15 mm, and an overall length of 100 mm. The tube is of 99.95% purity and is purchased from the Goodfellow Company. The microtube geometry is chosen due to its simplicity in fabrication and relative ease of modeling with detailed chemistry and transport properties. The central 70 mm of the microtube is resistively heated to achieve catalytic ignition. Three thermocouples (labeled TC1, TC2, and TC3) are spot-welded to the outside surface of the tube at distances of 29, 50, and 71% of the entire tube length. This corresponds to locations which are 20, 50, and 80% of the total heated section of the tube. The thermocouples are used as indications of the heating history of the tube as well as indications of exothermic reactions within the tube. Two nickel tabs are soldered to the tube and are used as attachment points to two ceramic posts. The ceramic insulators are mounted to an aluminum plate which is fixed inside a vacuum chamber. One pressure transducer is used to measure the inlet pressure of the tube, and another pressure transducer is used to measure the ambient pressure of the chamber.

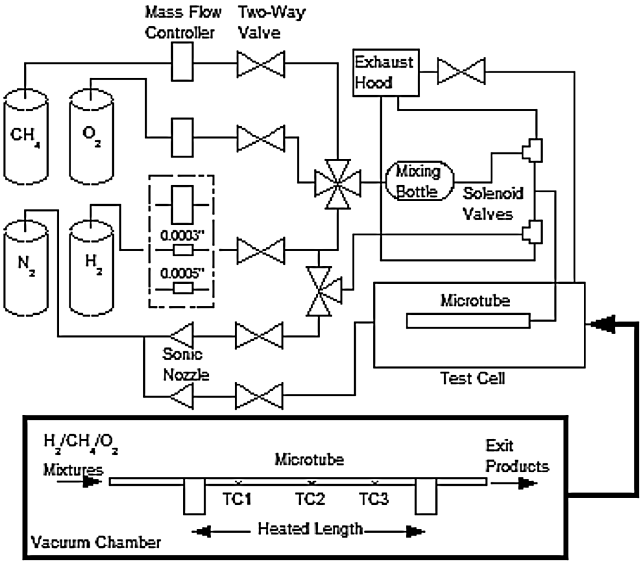

Fig. 1 Schematic of experimental setup.

The gas flow into the tube is controlled by three Unit Instruments mass flow controllers, one each for oxygen, methane, and high flow rates of hydrogen, whereas two different orifices with diameters of 0.0005 and 0.0003 in. are used when smaller flow rates of hydrogen are required. The accuracy for each mass flow controller is $\pm 1.5\%$ of full scale. Each mass flow controller is factory-calibrated for specific use with a particular reactant. In addition, flow rate calibrations for all mass flow controllers and sonic nozzles are further conducted in the lab using the bubble meter method. The reactants are premixed in a mixing bottle before entering the microtube, and a capability is added so that nitrogen could be fed into the tube before and after each experimental run so as to purge the tube. For data collection, a National Instruments SCXI-1000 chassis is used to acquire signals from the thermocouples, pressure transducers, and leads that measure the voltage across the heated section of the microtube.

III. Results and Discussion

The experimental results in this section consist of measurements of critical ignition temperatures, self-sustaining temperatures, and estimations of microtube performance parameters which include thrust, specific impulse, and power requirements. The effect of equivalence ratio and flow rate on the parameters of interest is investigated, and a detailed study of the effect of hydrogen addition to methane/oxygen mixtures is performed. A single overall equivalence ratio of the mixture ϕ is defined herein by considering the hydrogen and methane to be part of a two-component fuel. If we define the hydrogen addition parameter ξ as the molar fraction of hydrogen in the combined hydrogen and methane fuel, the mixture molar composition is then $\phi[(1-\xi)CH_4 + \xi H_2]$ for the fuel and $(2-1.5\xi)O_2$ for the oxidizer.

A detailed study of hydrogen addition to methane/oxygen mixtures is performed using a 0.40 mm platinum tube. The amount of hydrogen addition ranges from 0 ($\xi = 0$) to 100% ($\xi = 1$). From $\xi = 0$ to $\xi = 0.1$, a number of small increments in hydrogen addition is used, whereas above $\xi = 0.1$, larger increments of hydrogen addition are taken. Four different flow rates are investigated, one at a constant volumetric flow rate of $\dot{V} = 251$ SCCM (standard cubic centimeters per minute), and three at constant mass flow rates of $\dot{m} = 0.002$, 0.004, and 0.006 g/s. The constant mass flow rates are chosen based on desired thrust ranges and the allowable ranges of the mass flow controllers/sonic nozzles available.

At the start of the experiment, premixed gases are sent through the tube at room temperature and, a short time later, a small voltage is

[¶]Data available online at http://nssdc.gsfc.nasa.gov/planetary/mars/marssurf.html [retrieved 30 Nov. 2008].

applied across the middle section of the tube. Once a steady-state temperature profile across the tube is reached, the voltage is increased so that a new steady-state profile is achieved. The voltage ramp is performed in small stepwise voltage increments so as not to overshoot the ignition point. This process is repeated until the critical ignition point of the reactant mixture over platinum is reached at some point in the microtube. This process is illustrated in Fig. 2, which shows all thermocouple values as a function of time for a 20% ($\xi = 0.2$) hydrogen addition case of $\phi = 8$ and a mass flow rate of 0.002 g/s. A representative power supply voltage setting as a function of time is also overlaid over the temperature plot, so that it can be clearly determined whether a temperature rise is caused by the resistive heating of the tube or by exothermic reactions. Note that the power supply voltage shown here is the voltage measured directly from the dc power supply, which is different from the actual voltage across the microtube. Before ignition, the measured temperature of TC3 for this case always exhibits the highest local temperature, and thus ignition occurs close to the end of the microtube. Once ignition occurs, it is observed that TC1 and TC2 both increase in temperature and eventually surpass the temperature of TC3. The axial conductive heat transfer through the microtube walls could account for this upstream propagation of the reaction front. Once steady state is established, the voltage across the microtube is turned off, and it is seen that the thermocouple temperatures drop to new steady-state values. These are known as the self-sustaining temperatures, where the reactions inside the tube can sustain even though the power is no longer applied.

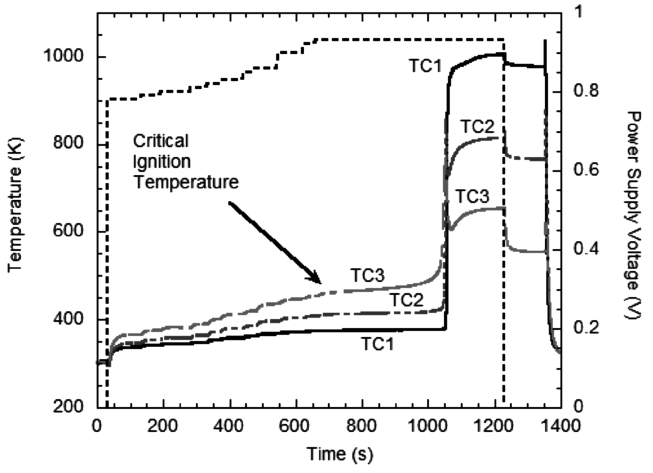

Fig. 2 Temperature profiles as a function of time for all three thermocouples, with $\phi = 8$, $\dot{m} = 0.002$ g/s, and $\xi = 0.2$. Reactant mixture is turned off at approximately 1350 s.

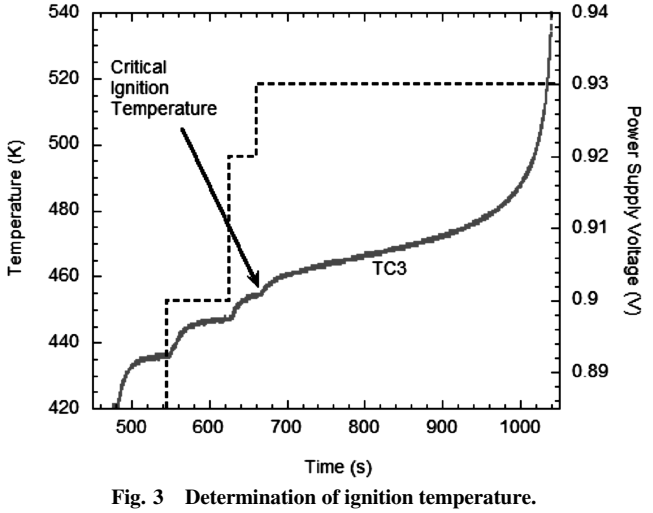

Fig. 3 Determination of ignition temperature.

Figure 3 overlays a plot of a representative heating history of the tube over an enlarged view of TC3. The graph illustrates how the steplike temperature increases are caused by the incremental change in voltage applied. The critical ignition temperature is defined herein as the last steady-state temperature value of TC3 before the last voltage increase is initiated. Thus, the critical ignition temperature is the measurable temperature of the tube at which a small amount of heat input increase will initiate ignition. The uncertainty in the ignition temperature measurement is estimated to be ± 8 K, based on the typical minimum temperature rise when the voltage is increased by the minimum allowable amount of 0.1 V.

A. General Trends

Figures 4 and 5 show all thermocouple values as a function of time for cases with 2% ($\xi = 0.02$) hydrogen addition and 15% ($\xi = 0.15$) hydrogen addition, respectively, with $\phi = 10$ and $\dot{V} = 251$ SCCM. A representative history of the power supply voltage is given as well to indicate when a change in temperature is caused by a change in the applied voltage.

For the case of 2% hydrogen addition, Fig. 4 shows a relatively large increase in temperature at all thermocouples once a small amount of heat is added to the tube at around 440 s into the experiment. Thus, this increase in temperature with only a small increase in applied heat flux is deemed the first ignition point and occurs at a temperature of 397 K. A steady-state value of 449 K is reached at TC3 after about 150 s. It is seen that there is a delay in the temperature

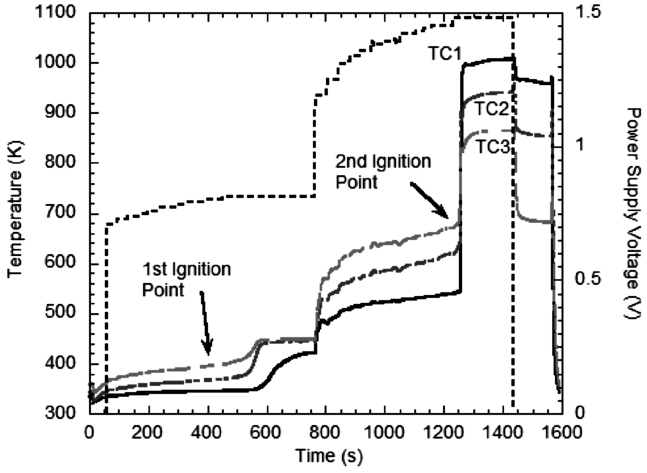

Fig. 4 Temperature profiles as a function of time for all three thermocouples, with 2% H_2 addition, $\phi = 10$, and $\dot{V} = 251$ SCCM.

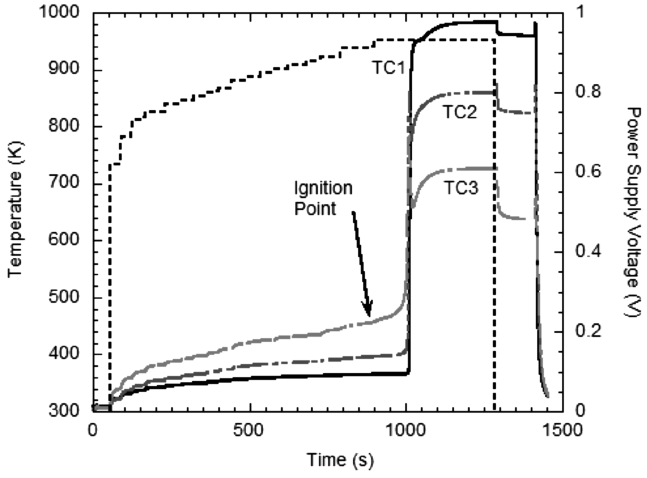

Fig. 5 Temperature profiles as a function of time for all three thermocouples, with 15% H_2 addition, $\phi = 10$, and $\dot{V} = 251$ SCCM.

increase of TC1. This can be attributed to the slow motion of the reaction front, which ignites downstream near TC3 and TC2 but then proceeds to propagate upstream toward TC1. After steady state is reached, resistive heating is once again applied to the tube, as indicated in Fig. 4. At approximately 1240 s, a very large temperature increase is seen at all thermocouples when a small increment of heat flux is applied to the tube. This is termed the second ignition temperature, and is found to be 670 K. TC1 shows the highest steady-state temperature after the second ignition, and thus the reaction front is assumed to be anchored in the upstream portion of the tube. The applied heat flux is shut off at 1440 s, and the steady-state self-sustaining temperature is shown to exist until the experiment is turned off.

Similar behavior is observed in experimental runs involving 3–7% hydrogen addition (not shown). Above 7% hydrogen addition, only one ignition point is observed. Figure 5 illustrates the nature of a one-ignition-point run with a 15% hydrogen addition case. Again, in this case, the catalytic reactions are self-sustained after turning off the applied heat flux at 1300 s.

B. Ignition Data

Figure 6a shows the resulting critical ignition data obtained for three different equivalence ratios at a volumetric flow rate of 251 SCCM as a function of hydrogen addition from 0 to 100%. For all cases, the individual reactant flow rates are varied to keep the total volumetric flow rate and equivalence ratio constant. Between 2–7% hydrogen addition, the lower critical ignition temperatures correspond to the first mild temperature rise observed experimentally, whereas the higher temperatures indicate onset of the second, larger temperature increase. It is seen that, at all levels of hydrogen addition, both the first ignition temperatures and second ignition temperatures are lower than that of a pure methane/oxygen mixture. This demonstrates that the addition of hydrogen facilitates methane/oxygen ignition at a lower preheat temperature.

It has been previously documented that the ignition temperature of methane/oxygen mixtures over platinum decreases with increasing equivalence ratio, whereas hydrogen/oxygen mixtures over a similar catalyst show the opposite trend [32]. For a methane/oxygen system, the higher sticking coefficient of oxygen in comparison to methane results in a catalyst surface initially covered with absorbed oxygen. With increasing equivalence ratio, less oxygen is absorbed on the catalyst surface, which allows for more open platinum sites to become available. These open platinum sites allow for more methane to be absorbed on the surface, facilitating an ignition at a lower temperature. However, hydrogen/oxygen mixtures show the opposite trend in that, with increasing equivalence ratio, hydrogen covers an increasing amount of the free platinum sites, which inhibits oxygen from absorbing to the surface. When examining the pure hydrogen and pure methane cases of Fig. 6a, this trend is also observed. It is also seen that, for 2–7% hydrogen addition, the first ignition point exhibits the same behavior as hydrogen/oxygen mixtures when the equivalence ratio is varied. However, the second ignition points in the same region show a decreasing ignition temperature as equivalence ratio is increased. Thus, it appears that the first ignition point corresponds to hydrogen reactions, and the second ignition point signifies the onset of methane oxidation.

A set of experimental runs is also performed with a constant mass flow rate of reactants into the microtube. This is carried out because thrust is directly proportional to mass flow rate, and thus fixing the inlet mass flow rate would yield more useful data about performance characteristics than a constant volumetric flow rate case. As the percentage of hydrogen in the fuel mixture is varied, the density of the inlet mixture changes. With a fixed mass flow rate and fixed inlet area, this implies that the inlet velocity also changes when the fuel mixture is varied. Thus, as the inlet velocity is varied, the residence time changes as well. With increasing hydrogen percentage, the density of the mixture decreases and thus the inlet velocity increases, leading to a lower residence time. In some cases studied herein, the residence time is not long enough for combustion to take place, and blowout extinction is observed.

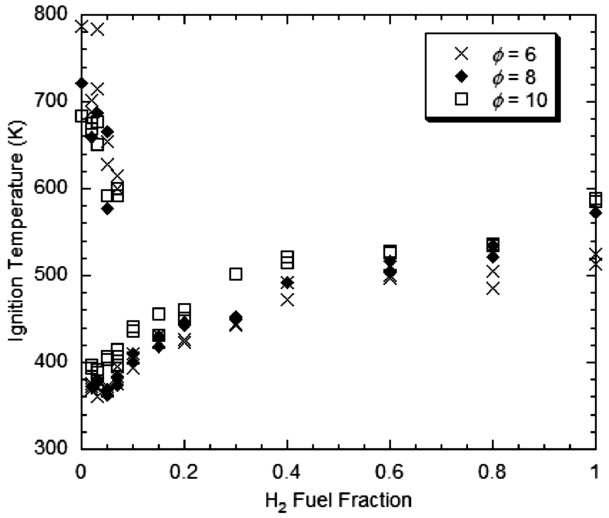

a) $\dot{V}$=251 SCCM

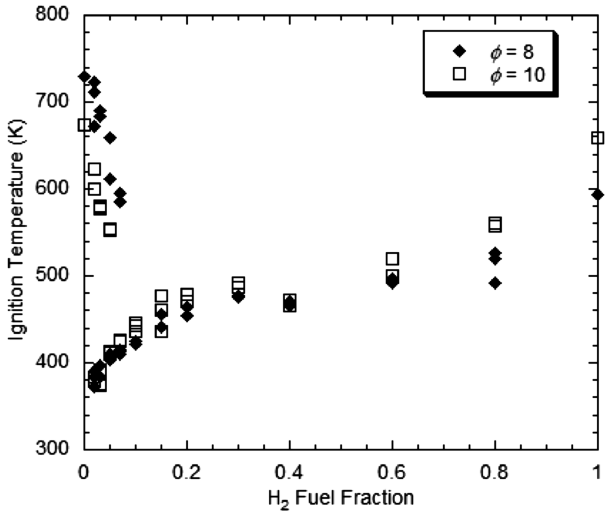

b) $\dot{m}$=0.002 g/s

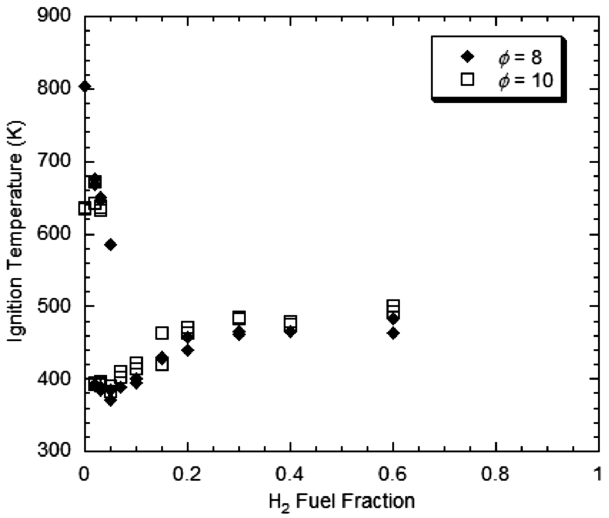

c) $\dot{m}$=0.006 g/s

Fig. 6 Ignition temperatures as a function of hydrogen addition at varying equivalence ratios and flow rates.

Figures 6b and 6c show critical ignition data for two different equivalence ratios at constant mass flow rates of 0.002 and 0.006 g/s, respectively. The results are similar to the constant volumetric flow rate case, with two ignition points present at low hydrogen additions

and the same trends with equivalence ratio. For the 0.006 g/s case shown in Fig. 6c, the mixture could not be ignited beyond hydrogen fuel fraction of $\xi = 0.6$, due to a small residence time within the tube.

C. Self-Sustaining Data

The self-sustaining steady-state temperature is determined by turning off the external heating supply once the system has reached an initial steady state after ignition. Almost all cases tested with a constant volumetric flow rate exhibit the ability to self-sustain catalytic reactions once the external heating is shut off. Figure 7a shows self-sustaining temperatures as measured by each thermocouple along the tube for the constant volumetric flow rate cases. For the pure methane cases ($H_2 = 0\%$), it is seen that the maximum temperature is recorded upstream of the tube at TC1, with the $\phi = 6$ case showing the highest temperature at 1020 K and the $\phi = 10$ case showing the lowest temperature at 917 K. Pure hydrogen ($H_2 = 100\%$) at $\phi = 6$ exhibits similar behavior, though at lower temperatures. The reactions within the tube fail to self-sustain for hydrogen at $\phi = 10$, presumably because the temperatures at such a high equivalence ratio are not high enough to overcome the heat losses to the environment.

Figure 7b shows the self-sustaining capability of pure methane mixtures at varying equivalence ratios and mass flow rates. The highest temperature occurs with the highest flow rate and lowest equivalence ratio, whereas the lowest temperature occurs at the lowest flow rate and highest equivalence ratio. For all cases, the reaction is anchored in the upstream portion of the tube. Figure 7c shows the self-sustaining temperatures of the 60% hydrogen addition cases. At the lowest mass flow rate of 0.002 g/s, the maximum temperature occurs at TC1, for 0.004 g/s, TC1 and TC2 are nearly equal, and for 0.006 g/s, TC2 exhibits the highest temperature. Thus, Fig. 7c shows how the reaction front is pushed downstream when the flow rate is increased.

D. Performance Characteristics

In addition to providing ignition and temperature properties of the microtube, other performance characteristics must be studied as well to aid in the development of methane/oxygen, hydrogen/oxygen, and methane/hydrogen/oxygen microthrusters for space-based applications. Two important parameters that are studied herein are the thrust and the specific impulse of the microtube. The power required for ignition is also investigated.

1. Thrust

The estimated thrust for a 0.40 mm platinum microtube at varying levels of methane/hydrogen ratio with a constant volumetric flow rate is shown in Fig. 8a. It is determined that, for the present vacuum test conditions, the flow is frictionally or/and thermally choked. At such conditions, the exit velocity is assumed to be sonic and the exit temperature is approximated as the steady-state value of TC3. The mean molecular weight and specific heat ratio are then estimated using a chemical equilibrium program. With all the exit conditions determined, the total thrust, including both momentum thrust and pressure thrust, can be calculated. The estimated uncertainty in the calculated thrust values is ± 0.06 mN.

It is seen from Fig. 8a that the maximum thrust achieved is 6.10 mN for a pure methane case with $\phi = 6$. For a $\phi = 8$ pure methane case, the estimated thrust is 5.80 mN, and, for a $\phi = 10$ case, the estimated thrust is 5.70 mN. Hence, the thrust values at pure methane are all very similar and do not vary much over the range of equivalence ratios tested. For pure hydrogen, the maximum thrust measured is 1.40 mN at $\phi = 6$, whereas the lowest is 1.30 mN at $\phi = 10$. Again, there is not much dependence of equivalence ratio on the total thrust for the range tested. However, the thrust varies greatly with respect to hydrogen addition. For the second ignition cases, a linear decrease in thrust is seen as the hydrogen addition varies from 0 to 100%. The linear decrease can be attributed to both the linear decrease in exit pressure and the linear decrease in mass flow rate as the hydrogen addition is increased. In comparison, the steady-state temperature of TC3 does not change as drastically over the same conditions and hence contributes minimally to the difference in thrust values. In the two-stage ignition regime, the thrust generated by the first, milder ignition is smaller than that due to the second, stronger ignition, as expected.

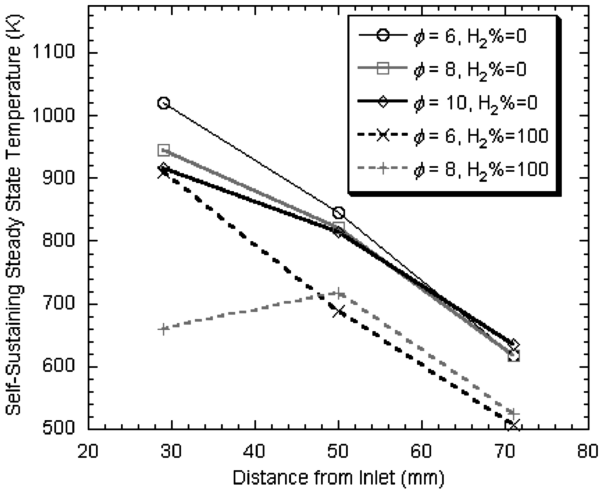

a) $\dot{V}$=251 SCCM

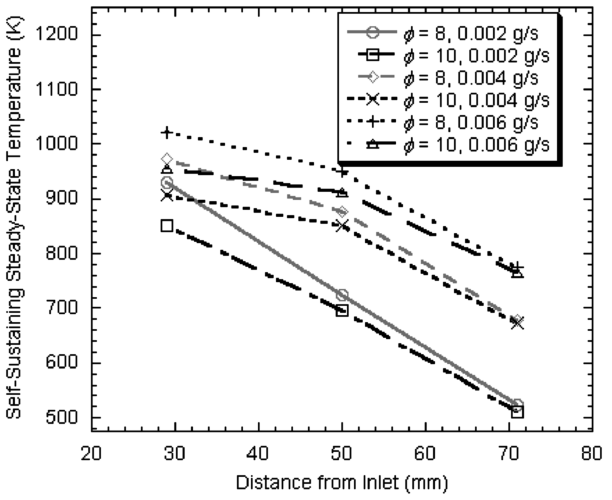

b) 0% H_2 addition

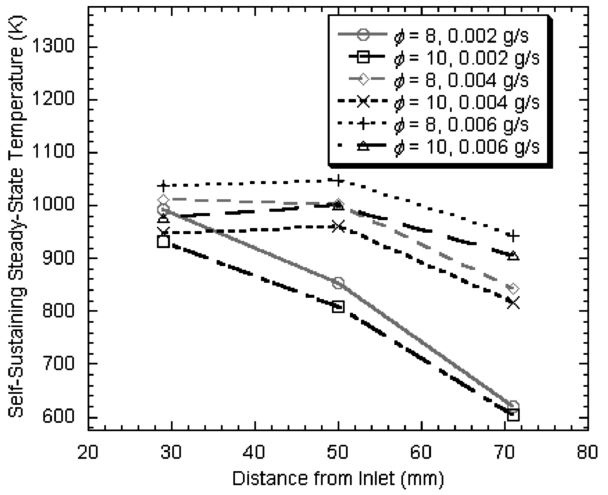

c) 60% H_2 addition

Fig. 7 Self-sustaining temperatures along the tube at varying equivalence ratios and flow rates.

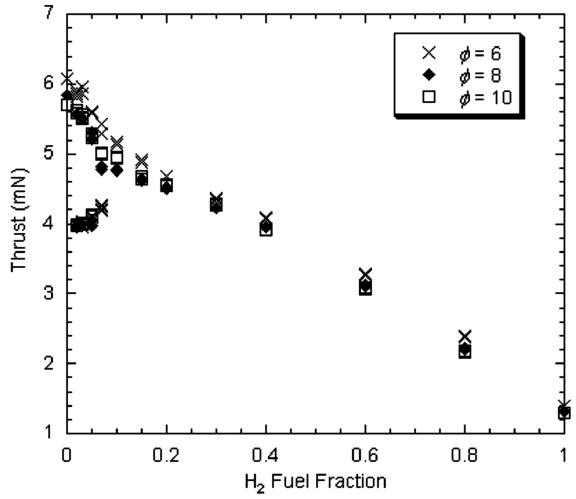

a) $\dot{V}$=251 SCCM

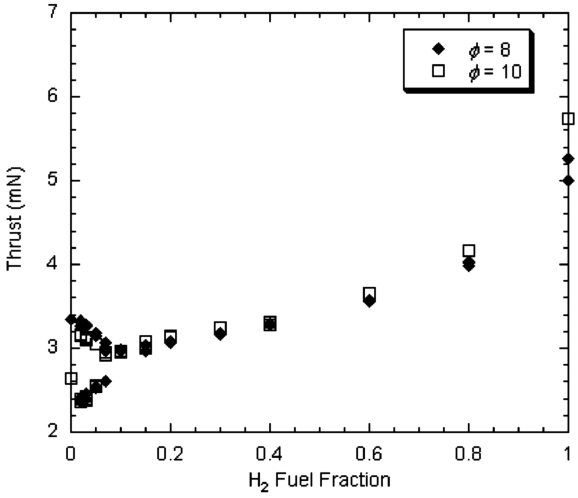

b) $\dot{m}$=0.002 g/s

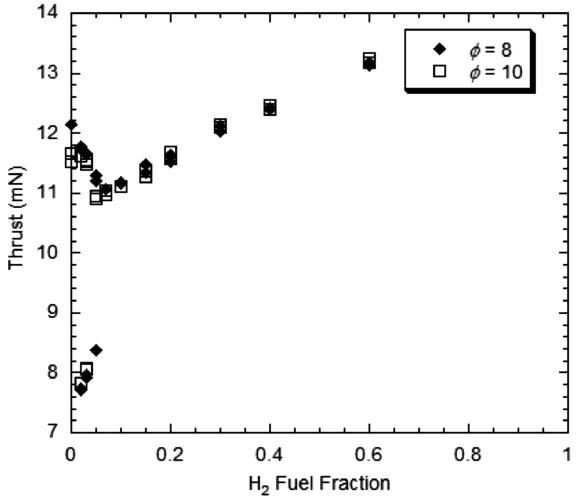

c) $\dot{m}$=0.006 g/s

Fig. 8 Thrust as a function of hydrogen fuel fraction at varying equivalence ratios and flow rates.

Thrust for constant mass flow rates of 0.002 and 0.006 g/s are seen in Figs. 8b and 8c, respectively. For the lower mass flow rate the range of thrust values are between 2–6 mN, whereas the thrust range for the higher flow rate is between 8–13 mN. There is a general increase in thrust as the hydrogen fuel fraction is increased for both mass flow rates. This can be attributed to the higher inlet velocity as more hydrogen is introduced into the mixture when the mass flow rate is kept constant.

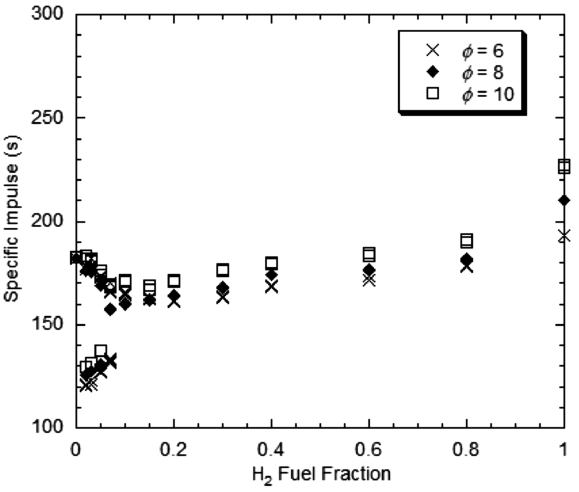

a) $\dot{V}$=251 SCCM

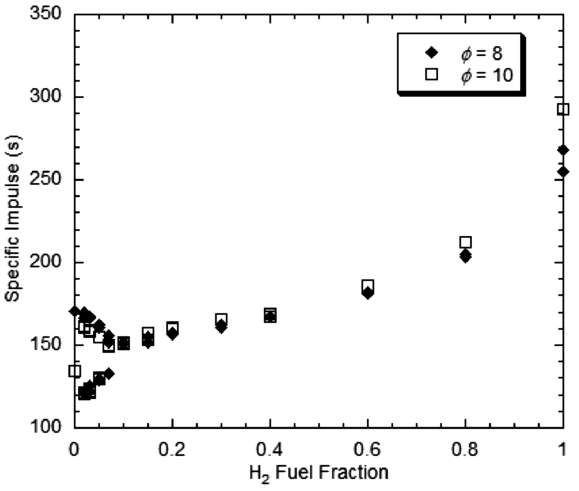

b) $\dot{m}$=0.002 g/s

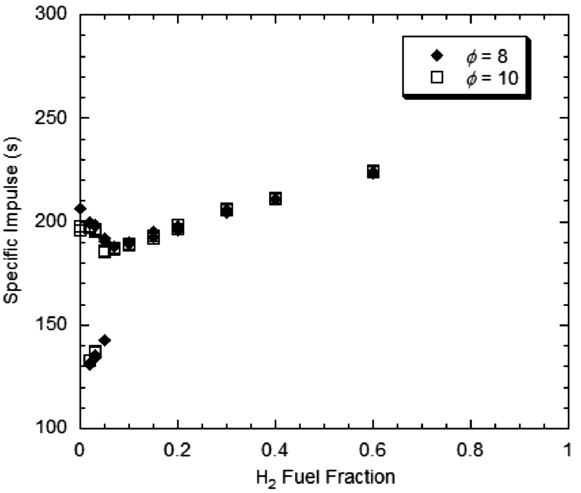

c) $\dot{m}$=0.006 g/s

Fig. 9 Specific impulse as a function of hydrogen fuel fraction at varying equivalence ratios and flow rates.

2. Specific Impulse

The specific impulse for a constant volumetric flow rate is shown in Fig. 9a. The estimated uncertainty in the calculated specific impulse values is ±10 s. As more hydrogen is added to the mixture, the mass flow rate into the tube and the product molecular weight both decrease; the specific impulse depends inversely on both of these parameters. At low hydrogen percentages, because the mass flow rate and product mixture composition are fairly constant, the decreasing temperature variation in TC3 is the dominant parameter, leading to the initial decrease in specific impulse for the second ignition cases until 10% H_2 addition. Whereas the temperature at TC3 past this point remains fairly constant, the inlet mass flow rate and mixture composition start to decrease at a rapid pace, which leads to higher specific impulses at higher hydrogen fuel fraction.

The specific impulses for two constant mass flow rates of 0.002 and 0.006 g/s are shown in Figs. 9b and 9c, respectively. For the lower mass flow rate, the range of specific impulse values is between 125–300 s. For the higher flow rate, because ignition is not possible beyond a hydrogen fuel fraction of $\xi = 0.6$, Fig. 9c shows that the specific impulse range is between 125–225 s. Because specific impulse is inversely proportional to molecular weight, more hydrogen in the fuel mixture favors a higher specific impulse, as seen in Fig. 9.

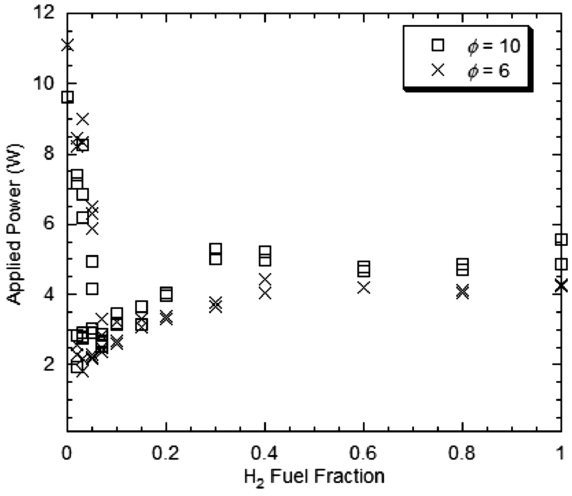

a) $\dot{V}$=251 SCCM

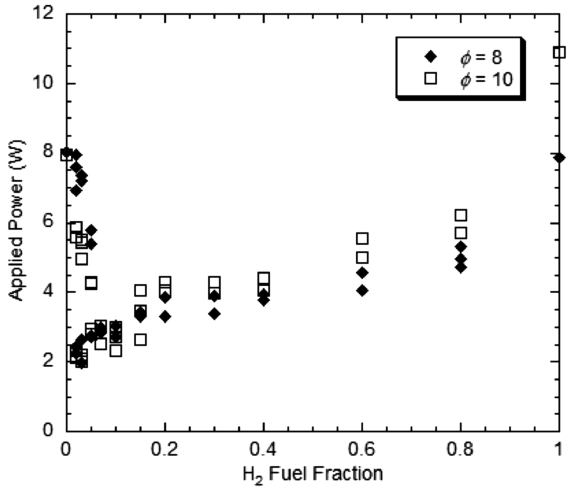

b) $\dot{m}$=0.002 g/s

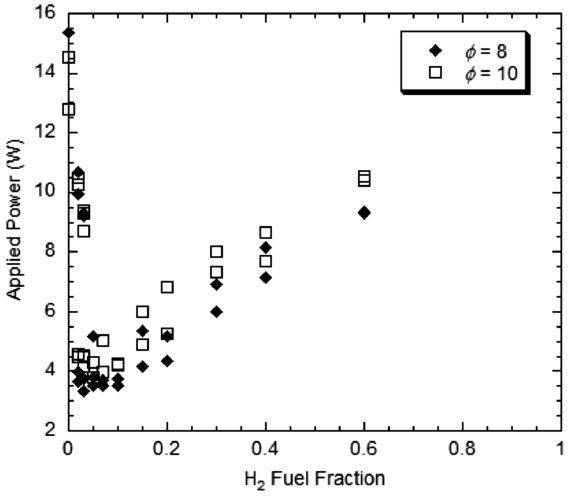

c) $\dot{m}$=0.006 g/s

Fig. 10 Applied power as a function of hydrogen fuel fraction at varying equivalence ratios and flow rates.

3. Power Requirements

Another important performance parameter is the power required to achieve ignition of methane/hydrogen/oxygen mixtures within the microtube. The main purpose of the hydrogen addition study is to lower the temperature for ignition and thus lower the power requirements needed for operation. Figure 10a summarizes the power needed to ignite the mixture as a function of hydrogen addition for a constant volumetric flow rate. The power is calculated based on the voltage measured across the tube just before ignition occurs and the resistance of the tube. For methane/oxygen mixtures, the power required for ignition is between 9–11 W, whereas the power required for hydrogen/oxygen mixtures is between 4–6 W. For low hydrogen additions, the first ignition point requires very small amounts of power, between 2–4 W, whereas the second ignition point requires between 5–10 W. Thus, the power needed to ignite fuel mixtures in the microtube is effectively lowered while still maintaining reasonable thrust and specific impulse values, as shown in the previous sections.

The power required to ignite methane/hydrogen/oxygen mixtures for a constant mass flow rate of 0.002 g/s is shown in Fig. 10b. The power required between 15–80% hydrogen addition is relatively constant, with a slightly increasing trend. In this region, the power is considerably less than that of a pure methane mixture. In this case, the power needed to ignite a pure hydrogen mixture is equal to or higher than a pure methane mixture. This may be because the residence time of the mixture is close to the critical residence time, and thus more power is required to ignite the mixture.

Figures 10c shows the power requirements of constant mass flow rates of 0.006 g/s. The lowest power requirements are seen around the first ignition point regime, and, for a single ignition point, the 10% hydrogen addition case exhibits the lowest power requirements. There is a linear increase in the power required after 10% hydrogen addition, and, in this high mass flow rate case, the higher hydrogen content cases (>60% hydrogen addition) could not be ignited.

IV. Conclusions

The utilization of chemical microthrusters for propulsion applications has been held back by the difficulties of achieving sustained combustion within a chemical micropropulsion device. The challenges include overcoming low residence times, substantial heat losses, and detrimental frictional effects as the chamber dimension is reduced. Because catalytic combustion is favored with a high surface-to-volume ratio, a catalyst can be used in sustaining reactions of fuels at the small scale, thus enabling chemical micropropulsion to become feasible. This study demonstrates this feasibility using a 0.40-mm-inside-diam platinum microtube as a model of a microthruster, using methane and hydrogen as fuels.

Hydrogen addition to fuel-rich methane/oxygen mixtures is used to lower the ignition temperature of the entire mixture, and the full range of addition from 0 to 100% is explored. The results confirm that, at any amount of hydrogen addition, the ignition temperature

could be effectively lowered when compared to a pure methane/oxygen mixture. Two-stage ignition phenomena are observed for low levels of hydrogen addition (2–7% by volume). After ignition, the power applied to the tube is turned off and self-sustainment of the reactions is observed in nearly all cases. Performance parameters such as thrust, specific impulse, and power required are evaluated. The thrust ranges obtained during the experiments are between 1–13 mN, whereas the specific impulse ranges between 125–300 s. These values are in the expected range of requirements for future chemical microthrusters.

Acknowledgments

This work was supported by the NASA Microgravity Combustion Program with Merrill King as contract monitor. The first author would also like to acknowledge fellowship support by the NASA Graduate Student Researchers Program.

References

[1] Baker, M. A., Curiel, A. S., Schaffner, J., and Sweeting, M., "'You Can Get There from Here:' Advanced Low Cost Propulsion Concepts for Small Satellites Beyond LEO," *Acta Astronautica*, Vol. 57, Nos. 2–8, 2005, pp. 288–301. doi:10.1016/j.actaastro.2005.03.046

[2] Mueller, J., "Thruster Options for Microspacecraft: A Review and Evaluation of State-of-the-Art and Emerging Technology," *Micropropulsion for Small Spacecraft*, edited by M. Micci and A. Ketsdever, Progress in Astronautics and Aeronautics, AIAA, Reston, VA, 2000, pp. 45–137.

[3] Lee, R. H., Lilly, T. C., Muntz, E. P., and Ketsdever, A. D., "Free Molecule Micro-Resistojet: Nanosatellite Propulsion," AIAA Paper 2005-4073, 2005.

[4] Lee, R. H., Bauer, A. M., Killingsworth, M. D., Lilly, T. C., Duncan,J. A., and Ketsdever, A.D., "Performance Characterization of the Free Molecule Micro-Resistojet Utilizing Water Propellant," AIAA Paper 2007-5185, 2007.

[5] Biagioni, L., Ceccanti, F., Saverdi, M., and Saviozzi, M., "Qualification Status of the FEEP-150 Electric Micropropulsion Subsystem," AIAA Paper 2005-4261, 2005.

[6] Mukerjee, E. V., Wallace, A. P., Yan, K. Y., Howard, D. W., Smith, R. L., and Collins, S. D., "Vaporizing Liquid Microthruster," *Sensors and Actuators A: Physical*, Vol. 83, Nos. 1–3, 2000, pp. 231–236. doi:10.1016/S0924-4247(99)00389-1

[7] Blandino, J., McDevitt, M., Mueller, J., Bame, D., and Green, A., "Characterization of Dryout Point in the Vaporizing Liquid Microthruster," *Journal of Propulsion and Power*, Vol. 22, No. 3, 2006, pp. 677–683. doi:10.2514/1.16179

[8] Smirnov, A. N., Raitses, Y., and Fisch, N. J., "Electron Cross-Field Transport in a Miniaturized Cylindrical Hall Thruster," *IEEE Transactions on Plasma Science*, Vol. 34, No. 2, 2006, pp. 132–141. doi:10.1109/TPS.2006.872185

[9] Simon, D. H. and Land, H. B., "Instrumentation Development for Micro Pulsed Plasma Thruster Experiments," AIAA Paper 2005-4264, 2005.

[10] Keidar, M., Boyd, I. D., Antonsen, E. L., Burton, R. L., and Spanjers, G. G., "Optimization Issues for a Micropulsed Plasma Thruster," *Journal of Propulsion and Power*, Vol. 22, No. 1, 2006, pp. 48–55. doi:10.2514/1.13954

[11] Ziemer, J. K., Gamero-Castaño, M., Hruby, V., Spence, D., Demmons, N., McCormick, R., Roy, T., and Gasdaska, C., "Colloid Micro-Newton Thruster Development for the ST7-DRS and LISA Missions," AIAA Paper 2005-4265, 2005.

[12] Alexander, M. S., Stark, J., Smith, K. L., Stevens, B., and Kent, B., "Electrospray Performance of Microfabricated Colloid Thruster Arrays," *Journal of Propulsion and Power*, Vol. 22, No. 3, 2006, pp. 620–627. doi:10.2514/1.15190

[13] Platt, D., "A Monopropellant Milli-Newton Thruster System for Attitude Control of Nanosatellites," *16th Annual USU Conference on Small Satellites*, SSCO2-VII-4, Utah State Univ. Research Foundation, North Logan, UT, 2002.

[14] Vieira, R., Bastos-Netto, D., Ledoux, M. J., and Pham-Huu, C., "Hydrazine Decomposition over Iridium Supported on Carbon Nanofibers Composite for Space Applications: Near Actual Flight Conditions Tests," *Applied Catalysis A: General*, Vol. 279, Nos. 1–2, 2005, pp. 35–40. doi:10.1016/j.apcata.2004.10.008

[15] London, A. P., Ayon, A. A., Epstein, A. H., Spearing, S. M., Harrison, T., Peles, Y., and Kerrebrock, J. L., "Microfabrication of a High Pressure Bipropellant Rocket Engine," *Sensors and Actuators A: Physical*, Vol. 92, Nos. 1–3, 2001, pp. 351–357. doi:10.1016/S0924-4247(01)00571-4

[16] Boyarko, G. A., Sung, C. J., and Schneider, S. J., "Catalyzed Combustion of Bipropellants for Micro-Spacecraft Propulsion," AIAA Paper 2003-4924, 2003.

[17] Boyarko, G. A., Sung, C. J., and Schneider, S. J., "Catalyzed Combustion of Hydrogen-Oxygen in Platinum Tubes for Micro-Propulsion Applications," *Proceedings of the Combustion Institute*, Vol. 30, No. 2, 2005, pp. 2481–2488. doi:10.1016/j.proci.2004.08.203

[18] Volchko, S. J., Sung, C. J., Huang, Y., and Schneider, S. J., "Catalytic Combustion of Rich Methane/Oxygen Mixtures for Micropropulsion Applications," *Journal of Propulsion and Power*, Vol. 22, No. 3, 2006, pp. 684–693. doi:10.2514/1.19809

[19] Rossi, C., Larangot, B., Lagrange, D., and Chaalane, A., "Final Characterizations of MEMS-based Pyrotechnical Microthrusters," *Sensors and Actuators A: Physical*, Vol. 121, No. 2, 2005, pp. 508–514. doi:10.1016/j.sna.2005.03.017

[20] Zhang, K. L., Chou, S. K., and Ang, S. S., "Performance Prediction of a Novel Solid-Propellant Microthruster," *Journal of Propulsion and Power*, Vol. 22, No. 1, 2006, pp. 56–63. doi:10.2514/1.6893

[21] Mungas, G. S., Das, D. K., and Kulkarni, D., "Design, Construction and Testing of a Low-Cost Hybrid Rocket Motor," *Aircraft Engineering and Aerospace Technology*, Vol. 75, No. 3, 2003, pp. 262–272.

[22] Kappenstein, C., Batonneau, Y., and Ford, M., "Chemical Micropropulsion: State of the Art and Catalyst Surface Requirements," AIAA Paper 2005–3920, 2005.

[23] Yetter, R. A., Yang, V., Wu, M. H., Wang, Y. X., Milius, D., Aksay, I. A., and Dryer, F. L., "Combustion Issues and Approaches for Chemical Microthrusters," *Advancements in Energetic Materials and Chemical Propulsion*, edited by K. K. Kuo, and J. D. Rivera, Begell House, Redding, CT, 2007, pp. 389–420.

[24] Fernandez-Pello, A. C., "Micropower Generation Using Combustion: Issues and Appraoches," *Proceedings of the Combustion Institute*, Vol. 29, No. 1, 2002, pp. 883–899. doi:10.1016/S1540-7489(02)80113-4

[25] Chao, Y. C., Chen, G. B., Hsu, C. J., Leu, T. S., and Wu, C. Y., "Operational Characteristics of Catalytic Combustion in a Platinum Microtube," *Combustion Science and Technology*, Vol. 176, No. 10, 2004, pp. 1755–1777. doi:10.1080/00102200490487599

[26] Sridhar, K. R., Finn, J. E., and Kliss, M. H., "In-Situ Resource Utilization Technologies for Mars Life Support Systems," *Advances in Space Research*, Vol. 25, No. 2, 2000, pp. 249–255. doi:10.1016/S0273-1177(99)00955-2

[27] Sridhar, K. R., Iacomini, C., and Finn, J. E., "Combined H2O/CO2 Solid Oxide Electrolysis for Mars In Situ Resource Utilization," *Journal of Propulsion and Power*, Vol. 20, No. 5, 2004, pp. 892–901. doi:10.2514/1.3480

[28] Deutschmann, O., Maier, L. I., Riedel, U., Stroemman, A. H., and Dibble, R. W., "Hydrogen Assisted Catalytic Combustion of Methane on Platinum," *Catalysis Today*, Vol. 59, Nos. 1–2, 2000, pp. 141–150. doi:10.1016/S0920-5861(00)00279-0

[29] Cimino, S., Di Benedetto, A., Pirone, R., and Russo, G., "CO, H_2, or C_3H_8 Assisted Catalytic Combustion of Methane over Supported $LaMnO_3$ Monoliths," *Catalysis Today*, Vol. 83, Nos. 1–4, 2003, pp. 33–43. doi:10.1016/S0920-5861(03)00214-1

[30] Hsu, H. W., "The Characteristics of Hydrogen-Assisted Catalytic Ignition of Methane," Ph.D. Dissertation, National Cheng Kung Univ., Tainan, Taiwan, ROC, 2004.

[31] Norton, D. G., and Vlachos, D. G., "Hydrogen Assisted Self-Ignition of Propane/Air Mixtures in Catalytic Microburners," *Proceedings of the Combustion Institute*, Vol. 30, No. 2, 2005, pp. 2473–2480. doi:10.1016/j.proci.2004.08.188

[32] Deutschmann, O., Schmidt, R., Behrendt, F., and Warnatz, J., "Numerical Modeling of Catalytic Ignition," *Proceedings of the Combustion Institute*, Vol. 26, No. 1, 1996, pp. 1747–1754.

T. Lieuwen
Associate Editor